Available online at www.sciencedirect.com
ScienceDirect
Journal of the European Ceramic Society 30 (2010) 3093–3101
www.elsevier.com/locate/jeurceramsoc

Characterization by acoustic emission pattern recognition of microstructure evolution in a fused-cast refractory during high temperature cycling

C. Patapy [a], A. Proust [b], D. Marlot [b], M. Huger [a], T. Chotard [a,*]

[a] *Groupe d'Etude des Matériaux Hétérogènes (GEMH), EA 3178 - 47-73 avenue Albert Thomas, 87065 Limoges, France*
[b] *Euro Physical Acoustics SA, 27 rue Magellan, 94370 Sucy en Brie, France*

Received 15 January 2010; received in revised form 9 March 2010; accepted 15 March 2010
Available online 3 August 2010

Abstract

Fused-cast refractory materials are widely used in the glass industry, especially in the building of superstructures and side walls of fusion furnaces. The HZFC (High Zirconia Fused Cast) products are especially used as tank blocks for the fusion of highly corrosive glasses melted at very high temperature (such as LCD glass), due to their high corrosion resistance and their low generation of glass defects generation.

The presence of this high amount of pure ZrO_2 in the refractory can be responsible for microdamage occurrence during the cooling step after melt casting (annealing), associated to the martensitic transition of zirconia.

Acoustic emission (AE) analysis is well known as a reliable tool to investigate microstuctural evolution at a very small scale. In this work, a fused-cast ZrO_2 refractory has been investigated using a AE unsupervised pattern recognition procedure and a frequency-energy coupled analysis. Data gathering during thermal cycles at high temperature (typically 1500 °C) has been done thanks to an innovative self-developed testing device. The analysis of frequency and energy parameters makes it possible to detect and to characterize the occurrence and the chronology of microdamage in specific range of temperature. Hypothesis concerning different ways of microdamage formation below the temperature of the martensitic transformation of ZrO_2 during the cooling stage can be proposed related to thermo-mechanical properties and the microstructure of the material. In particular, intergranular and intragranular microcracks due to CTE mismatches occurring in the material have been also investigated.

Keywords: ZrO_2; Refractories; Damage characterization; Mechanical properties

1. Introduction

High technology applications such as LCD devices need special glasses with a very high purity favor to avoid defects. Refractories with a very high content of zirconia are currently used for the melting of these glasses. In fact, several studies show that ZrO_2 shows a remarkable resistance against corrosion.[1,2] But the difficulties to fabricate such materials due to the martensitic transformation of zirconia and its associated volume change are responsible for many studies.[3–5] They aim to develop a composition which limits the thermo-mechanical stresses and microcracking induced by the critical manufacturing steps especially the controlled cooling step after casting. However, we can notice that this initial damage is mainly recovered at operating temperature.

Acoustic emission is a useful technique applied commonly in the building domain to assess the integrity of structures like bridges or dams.[6] Since more than 20 years, it has been developed to investigate microstructure phenomena which can appear due to phase transformations or damage occurrence in materials. These studies are often performed on composites at room temperature due to the impossibility to use piezoelectric sensors above 550 °C. Studying heterogeneous materials like refractories at temperatures up to 1500 °C by acoustic emission is then an innovative genuine approach to understand damage mechanisms and to correlate thermo-mechanical properties with microstructure.

The present paper aims to study a fused-cast refractory based on a boron glassy phase by characterizing microdamage mechanisms, in particular the ones induced by the martensitic transition

* Corresponding author.
E-mail addresses: cedric.patapy@etu.unilim.fr (C. Patapy), Aproust@epandt.com (A. Proust), marc.huger@unilim.fr (M. Huger), thierry.chotard@unilim.fr (T. Chotard).

0955-2219/$ – see front matter © 2010 Elsevier Ltd. All rights reserved.
doi:10.1016/j.jeurceramsoc.2010.07.021

of ZrO_2. Acoustic emission monitoring is performed during thermal treatments at high temperature (up to 1500 °C) with an innovative testing device. The reliability and the efficiency of the device are first investigated. A pattern recognition non supervised method is applied to filter parasitic noise data. Finally, a frequency analysis of AE transients coupled with a signal energy investigation makes it possible to identify temperature domains related to microdamage occurrence during the cooling stage. This analysis helps us to make hypothesis concerning microstructure mechanisms chronology.

2. Materials

A HZ material (HZ-A), supplied by Saint-Gobain CREE, has been manufactured for this study. It shows a three dimensional inter-linked phase structure with dendrites, i.e. elongated crystals of zirconia embedded into the glassy phase. It contains 94 wt.% of monoclinic zirconia and 6 wt.% of a boron glassy phase (Fig. 1).

HZ-A presents the martensitic transformation from the tetragonal form of zirconia to the monoclinic one at around 1000 °C, during cooling. This transition is responsible for an important volume change (around 4%) and a large shear deformation (0.16%). The glassy phase plays then a major role to accommodate internal stresses induced by the anisotropic expansion mismatch between ZrO_2 grains during this transformation, even if intergranular microcracks are generated.

Besides, different monoclinic crystallographic equivalent structures can be created from one single tetragonal crystal which is responsible for twinning phenomena and intragranular microcracks.[7–9] Such entities can be seen in HZ-A by SEM in Back Scattering Electron mode using a special polishing preparation including colloidal silica (Fig. 2).

3. Acoutic emission at high temperature

Acoustic emission (AE) is defined as "the class of phenomena whereby transient elastic waves are generated by the rapid release of energy from localized sources within a material (or structure)". This technique is widely used to control the evolution of defects for structural quality monitoring. When a material is subjected to mechanical or thermal stresses, acoustic emission can be generated by a variety of damage mechanisms such as for example crack nucleation and propagation, cooperative dislocation motions, twinning, grain boundary sliding, Barkhausen effect (realignment or growth of magnetic domains), phase transformations in alloys without diffusion, fibre breakage in composite materials or inclusion fracture or twinning in metallic alloys.[10–13] Therefore, AE has been used to study microstructure evolutions and damage propagation. Studied materials are often characterized at ambient temperature due to experimental difficulties to set sensors in high temperature conditions. Other new applications of this technique have been recently developed.[14–17]

This study aims to study refractories, i.e. heterogeneous complex materials at high temperatures (typically up to 1500 °C). An original technique has been developed in the GEMH lab-

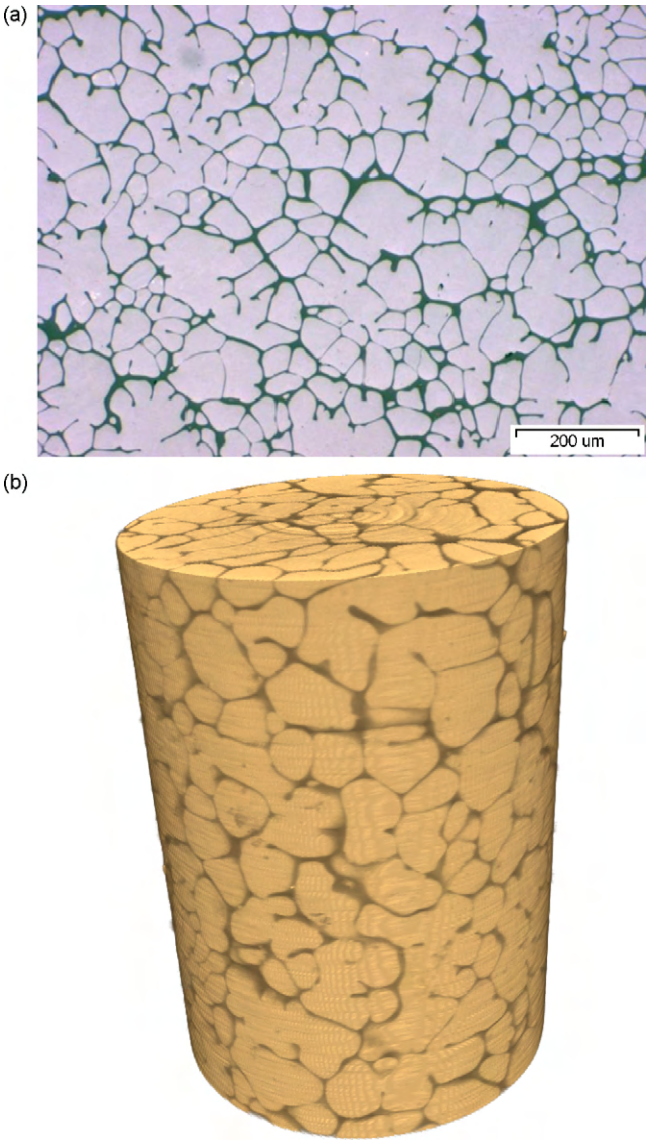

Fig. 1. SEM observation (a) and X-Ray microtomography picture (b) of HZ-A material.

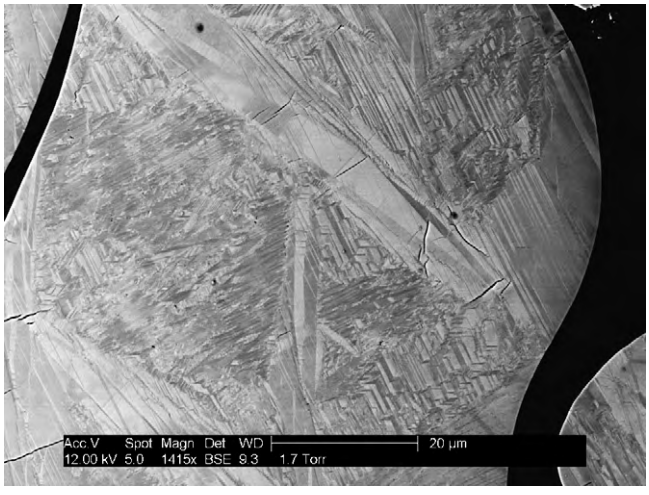

Fig. 2. ESEM observation of a HZ-A microstructure.

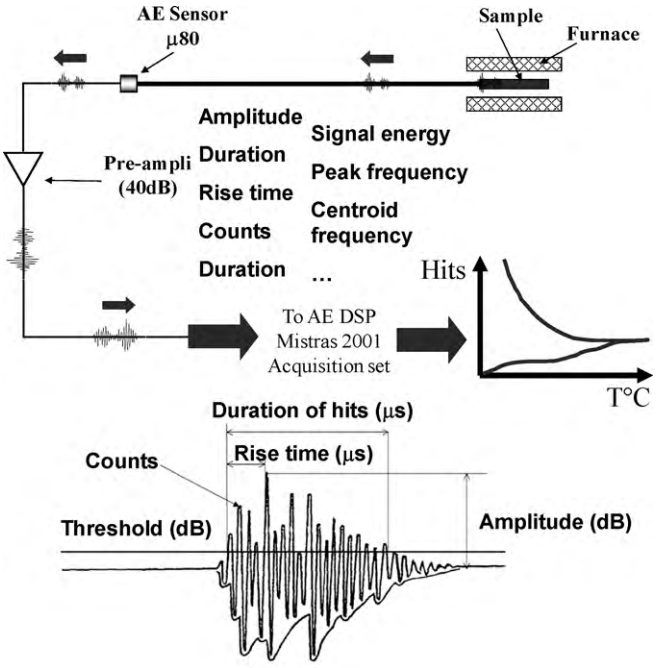

Fig. 3. High temperature acoustic emission device and main acoustic emission features.

oratory to monitor the in situ microstructure evolution at high temperature. A wide-band sensor (175 kHz–1 MHz) (PAC μ80), connected to a preamplifier (PAC 1220A), collects, through an alumina waveguide, the signal induced by the elastic waves released within the sample (5.5 mm × 5.5 mm × 25 mm). To avoid parasitic noises from coupling material phase transformation, a dry contact between the sample and the waveguide is set. A threshold of 40 dB_{EA} has been chosen in order to filter background noise. The signal is then amplified and treated by a Mistras 2001 acquisition device from Euro Physical Acoustics Company. This system processes the transients (hits) and extracts traditional features such as count, rise time, duration of hit, count to peak, amplitude (in dB_{EA}), energy and also in real time calculates frequency parameters, and records the waveforms. Fig. 3 represents a schematic of the AE experimental set-up. As only one sensor is used, each recorded signal will be called "hits" in opposite of the denominate "event" more likely used when the signal (localized) correlated by two sensors located on the structure.

AE data analysis is performed with a dedicated software (NOESIS, Europhysical Acoustics). The main objective of AE monitoring is to study the influence of the martensitic transformation on microdamage evolution during the cooling stage.

Descriptor-based acoustic emission methodologies often focus on time features, which are not sufficient to fully characterized AE from complex materials. Most studies only use amplitude and the energy of the signal to characterize damage propagation.[18–21] It has been shown by Ni[22] that overall frequency content of AE signals is almost unchanged while the amplitude is greatly attenuated with long distance propagation. Thus several studies using Short Time Fourier Transform (STFT)[23] and continuous wavelet transform (CWT) procedures[22,24–26] were performed to discriminate damage mechanisms in composites. A frequency analysis using the centroid frequency (f_c), i.e. a sum of magnitude times frequency spectrum divided by a sum of magnitude as equivalent to the first moment of inertia is performed here (Eq. (1)).[27] This frequency parameter is thus a frequency barycentre of the whole recorded signal.

$$f_c = \frac{\int_0^\infty fS(f)df}{\int_0^\infty S(f)df} \quad (1)$$

With f the frequency obtained for each point $S(f)$ of the FFT representation.

In fact, the AE sensor is often chosen in a theoretical way with regard to the type of source and function of the attenuation due to the propagation in the material. In the present case, the system is formed of the material itself and the associated waveguide. The first function of transfer to take into account is the one of the material and then the one of the waveguide. Thus, the signal given by the sensor shows a very resonant behavior. Frequency contents are very influenced by the characteristics of the material, the sensor response and that of the associated waveguide. Therefore, the calculus of the maximum of the energy spectral density (peak frequency) does not bring a lot of information. Thereby, the centroid frequency will be preferred here to characterize frequency components of the signal. An example of two signals with the same maximum of the Fourier transform and at the same time differences in centroid frequency (279 kHz for the signal on the left and 331 kHz for the signal on the right) is given in Fig. 4. The frequency evolution will be used in conjunction with cumulative signal energy analysis of the AE signals to advance microstructure hypothesis.

4. Results and discussion

4.1. Reliability of the testing device

Before investigating acoustic emission parameters, it is necessary to verify the reliability of the acoustic emission data. This very important part aims to show the ability of the acoustic emission device to obtain a rather good reproducibility of acoustic emission recording. Then, a clustering approach and filtering procedure are performed to improve the quality of data.

4.2. Evidence of a good reproducibility

Several tests have been performed on HZ-A material during three successive thermal cycles up to 1500 °C (dwell of 1 h) to look at the efficiency of data reproducibility using the high temperature testing device. The AE transient signal energy of the AE signal is linked to the nature of the phenomena responsible for the hit. Thereby, the cumulative signal energy versus temperature relative to the HZ-A material is plotted for two different tests in Fig. 5.

Evolution of cumulative AE signal AE energy is very similar for the two records. During thermal cycles, we can hypothesise that a large number of phenomena (microcracking, rubbing,

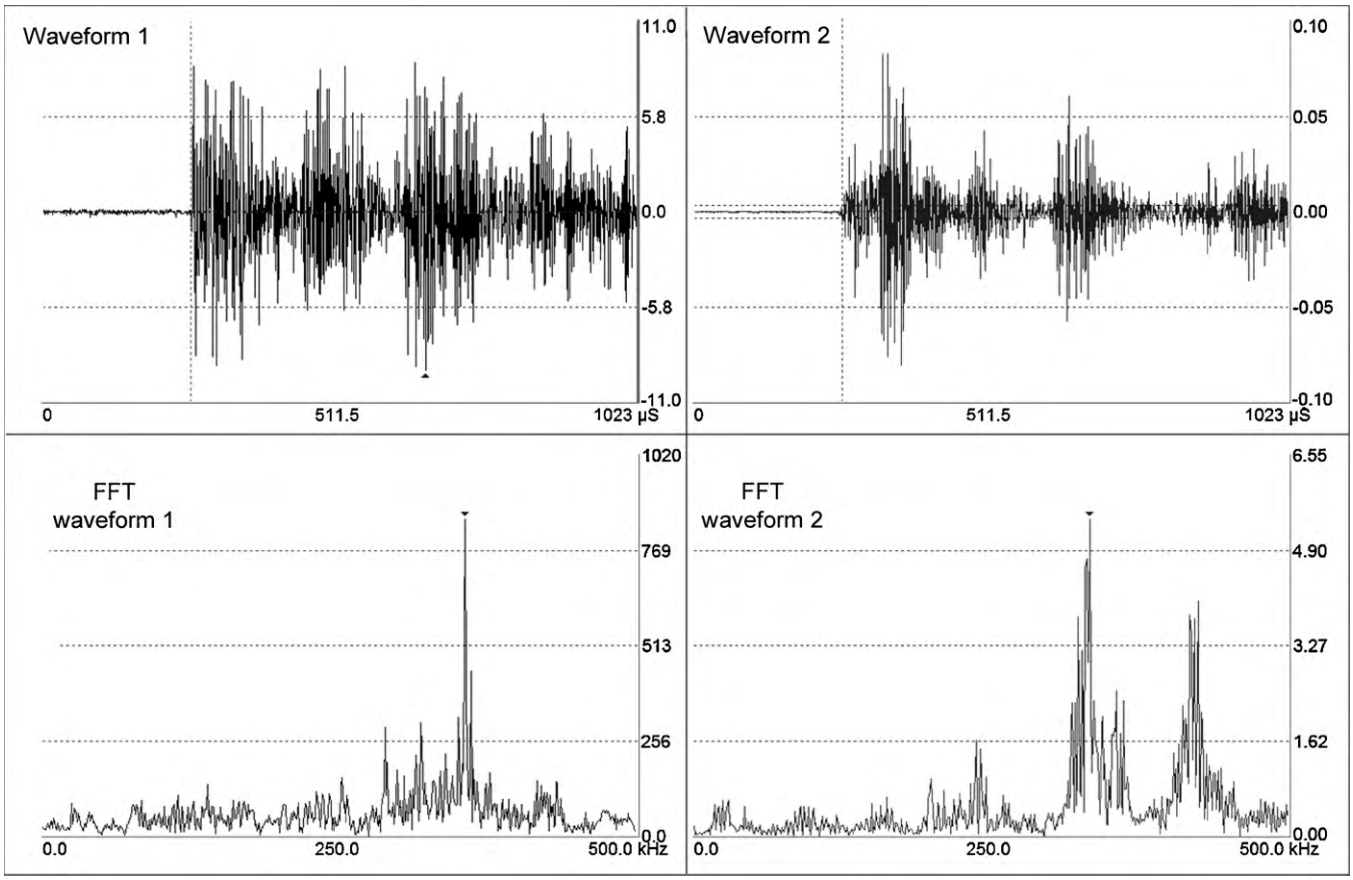

Fig. 4. Examples of AE signals with the same peak frequency and different centroid frequencies.

phase transformation,. . .) are involved. Each of them has its own signal energy distribution. Thus obtaining closer evolution of cumulative energy is the evidence of the very low part of parasitic signals in all the recorded data.

Despite the complexity of the studied materials and the number of successive thermal treatments, the experimental set-up makes it possible to obtain great reproducibility of data collection. As amplitude and signal energy parameters are obviously linked, another way to compare two experiments is to plot the distribution function (cumulative hits versus amplitude) for the two tests (Fig. 6). As the amplitude distributions are very close and the Henry slopes[28] are very similar we can conclude that from a statistical point of view the corresponding two tests are rather similar.

In order to be sure that we make a genuine time separation between hits and get a good discrimination of the echoes, we optimized the acquisition set up with the following time parameters (Peak Definition Time = 200 μs; Hit Definition Time = 1000 μs and Hit Lockout Time = 1000 μs).

Thus, the AE experimental device developed here is suitable to carry out a quantitative study. It avoids the most part of parasitic noises. Nonetheless, an unsupervised pattern recognition procedure has been developed to purge further residual parasitic data.

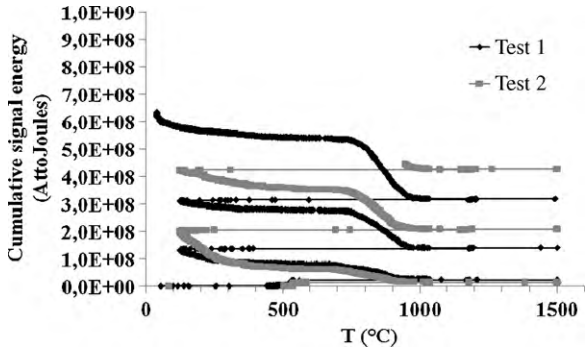

Fig. 5. Cumulative signal energy versus temperature during three successive thermal cycles up to 1500 °C (dwell 1 h).

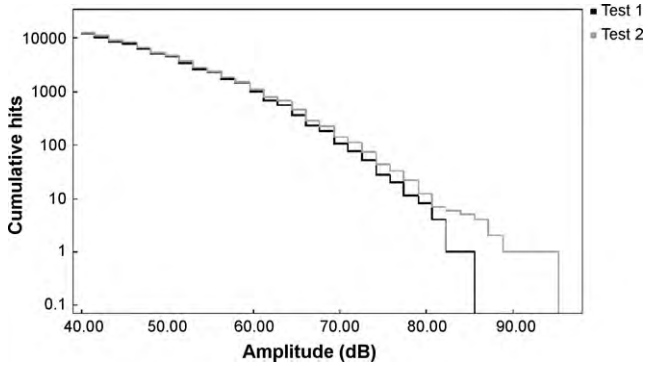

Fig. 6. Min–max distribution of cumulative hits versus amplitude profile for HZ-A.

4.3. Clustering approach and identification of parasitic noises

As the waveguide system acts as a filter, a pattern recognition approach is necessary to separate parasitic noises from the whole data. It needs an adequate evaluation of classification results to enhance the ability of quantifying the partitioning of datasets. Thereby, such an approach often consists in first defining an appropriate procedure for the extraction of the features associated with the waveforms. It allows selecting a limited number of waveform parameters to describe microstructural mechanisms. Then, data can be normalized, projected to their principal component axis and characterized by clustering (appropriate) algorithms. A classification of all waveforms within their similarities is so obtained.[29,30]

Statistic parameters, namely the Wilks lambda, R_{ij} and τ are used to describe the relevance of AE parameters.[31] The first one is widely used to illustrate the state of separation of clusters. It varies between 0 (waveforms classes are widely separated) and 1 (clusters are very close to each other). As the purpose is to create distinct groups, the lower the Wilk's lambda for a AE parameter is, the better the class separation. The two other parameters from Davies and Bow[32,33] are defined to evaluate more particularly the appropriate number of clusters to separate different kinds of AE waveforms. R_{ij} is relative to the average proximity of the clusters and τ is the measure for the mean spatial distribution of the clusters relative to each other. Besides, the clusters separate all the more as the values of R_{ij} and τ are respectively low and high. These variables are used in this study to evaluate the most discriminant AE parameters in the understanding of damage occurrence.

Identification of the most relevant AE features is first realized to help to distinguish different classes of signal. Statistic factors described above, i.e. Wilks lambda, R_{ij} and τ, have been computed to select representative AE features.

A clustering approach based in particular on a k-mean model[34] has been performed using a selection of the most discriminant parameters. Three particular classes have been extracted from all data. They will be called in the following part Class 1, Class 2 and Class 3. Contribution of these classes against all data is plotted in cumulative hits versus temperature (Fig. 7).

Hits associated to Classes 2 and 3 are less numerous than hits from Class 1. Nonetheless, any clear correlation with a special range of temperature is not seen. A deeper analysis of signal frequencies seems to show that Class 2 present very high frequency signals and Class 3 low frequency ones. Thereby, it suggests assuming that they are respectively electromagnetic parasitic and mechanical noise. The medium amplitude and relative high duration of hits belonging to Class 1 could be the potential signature of microcracks propagation.

The using of an unsupervised method is a good approach when signal parameters of mechanisms associated to the studied material are well known. Among the three classes of signals which have been isolated, two corresponds to parasitic noises and one to potential micro crack propagation. This approach is thus a good way to enhance the filtering process of undesirable

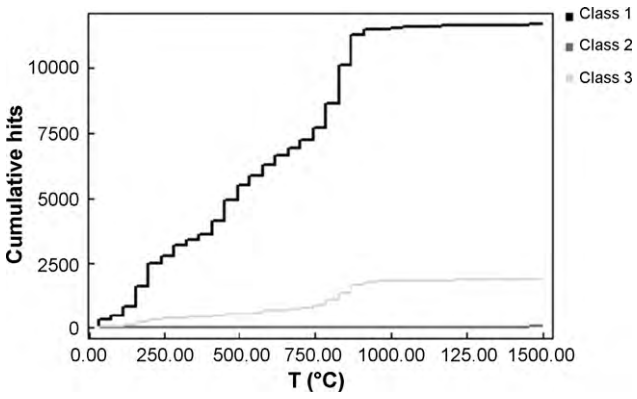

Fig. 7. Cumulative hits associated to each class versus temperature.

datasets. In the following part of the study, Classes 1 and 2 will be excluded.

4.4. AE analysis of the cooling stage

4.4.1. Thermo-mechanical properties

The present work aims to identify the temperature range of microdamage occurrence during the cooling stage. Before investigating AE data, Young's modulus measurements and thermal expansion measurements have been performed for the studied material (Fig. 8).

Two particular phenomena must be noticed concerning the thermal expansion curve:

- a large expansion on cooling at around 1000 °C due to the martensitic transformation of ZrO_2. This transition temperature is nearly exactly the tetragonal to monoclinic transition temperature of a single crystal of zirconia.
- a slope change of the thermal expansion curve at around 450 °C. The coefficient of thermal expansion seems to decrease below this temperature.

Young's modulus evolution of HZ-A during the cooling stage has been already discussed in a previous paper.[35] Four main steps were identified:

1. Domain 1: from 1500 °C, and down to the reverse T → M transformation at about 1000 °C, the Young's modulus

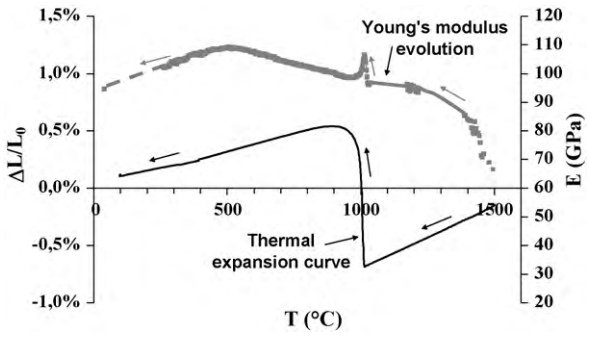

Fig. 8. Thermal expansion analysis and Young's modulus evolution during a cooling stage from 1500 °C.

increases in line with the viscosity of the glassy phase (rigidification). There is a narrow peak in E at the transformation temperature.
2. Domain 2: the Young's modulus slowly increases from 990 °C to 920 °C for HZ-A.
3. Domain 3: the regular increase of E remains at the same rate. The temperature range of this step is of 220 °C.
4. Domain 4: the linearity loss of E begins. This phenomenon takes place from 690 °C to 300 °C.
5. Domain 5: from 300 °C to room temperature, a rapid decrease of E is observed.

4.4.2. Frequency and energy analysis

Authors suggest to focus on two AE parameters: the centroid frequency and the signal energy parameters. First, a filtering procedure for all signals below 50 dB_{EA} is performed to improve the statistical efficiency of centroid frequency. The cooling process is divided into ranges of 100 °C. For each range, an average value of the fit centroid frequency is plotted. This value is an average of all centroid frequencies processed on this range of temperature during three successive thermal cooling stages. Besides, on each range, the cumulative value of AE signal energy associated to hits detected on this range of temperature for the same three successive cooling stages is calculated. Evolution of average values of centroid frequency and cumulative signal energy are plotted in Fig. 9. Besides, examples of different spectra with remarkable differences in energy and frequency centroid are given in Fig. 10 as an illustration. As the martensitic transformation of zirconia is considered to initiate microdamage, results only focus on what happens below 1000 °C.

Three main steps can be highlighted:

A: From 1000 °C to 700 °C, the centroid frequency rises up continuously. Cumulative signal energy increases significantly in the range 900–800 °C but falls down drastically in the next 100 °C range.
B: Both the centroid frequency and cumulative signal energy see progressively their values increasing in the zone 700–400 °C. Nonetheless, maximum values obtained are lower (strongly for signal energy) than they are at the maximum of the previous step.
C: From 400 °C to 100 °C, a relative dwell is observed for both parameters.

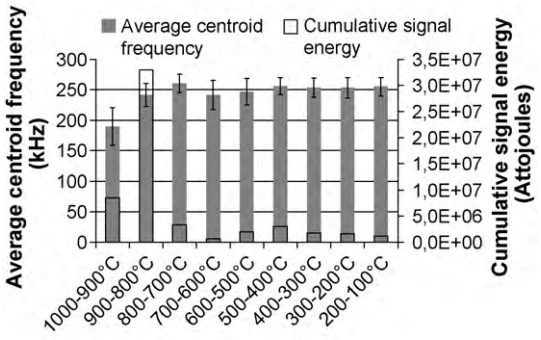

Fig. 9. Average centroid frequency and cumulative signal energy evolution during the cooling process (on each 100 °C temperature domains).

A first remark concerns the strong relationship which seems to exist between the centroid frequency and cumulative energy evolution. As these two parameters express microstructure mechanisms, it is clear that microdamage evolves in temperature.

It is more difficult to link these acoustic emission parameters to microdamage mechanisms. In fact, it requires a perfect knowledge of the transfer function of the device with the temperature and at the same time the ability to identify the correspondence of a microstructure phenomenon to a particular signal signature. Thereby, in the following part of the paper, only hypotheses will be suggested by comparison with thermo-mechanical tests.

4.4.3. Discussion

There is no doubt that the happening of the transformation of zirconia at around 1000 °C is responsible for microdamage occurrence through:

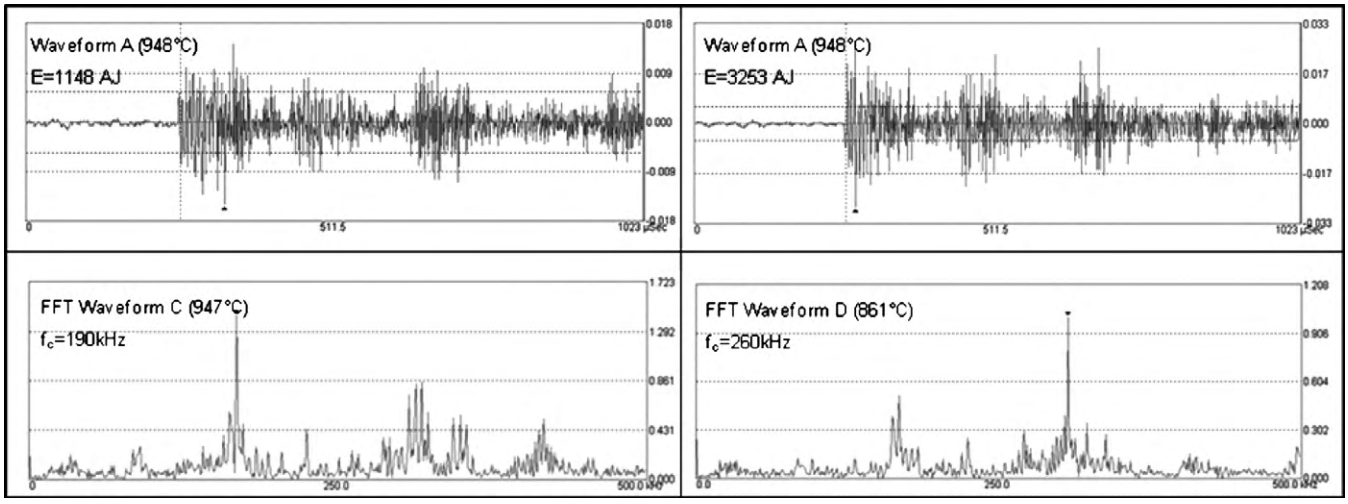

Fig. 10. Different AE signals with noticeable differences in energy and centroid frequency.

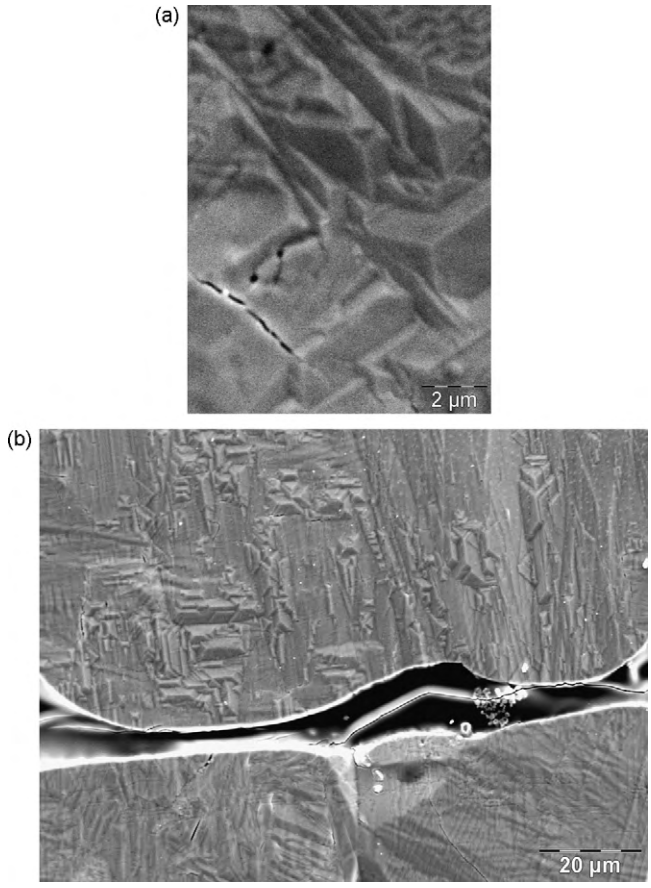

Fig. 11. Microcracking pattern of HZ-A heat treated at 1500 °C: a intragranular microcrack (a) and intergranular microcracks (b).

- the generation of monoclinic variants with CTE mismatches between them, creating twinning phenomena and intragranular microcracking along particular directions (Fig. 11a)
- a large expansion of the zirconia dendrites responsible for rubbing between zirconia grains and the glassy phase and between ZrO_2 grains themselves. Potential intergranular microcracks can be formed (Fig. 11b).

Besides, the classical effect of CTE mismatches between the glassy phase and zirconia grains and between ZrO_2 grains themselves (anisotropy of crystallographic axes) due to the cooling process is a source of intergranular microdamage for the first one and potential intragranular microcracks for the second one. Microstructure observations confirm both inter and intragranular microcracks.

Authors suggest separating the discussion into three temperature areas: a high temperature domain (1000–800 °C), a medium temperature area (800–400 °C) and a low temperature one (400–100 °C).

4.4.3.1. High temperature domain: 1000–700 °C. Measurements of viscosity evolution on glass synthetic samples with the same composition as the glassy phase of HZ-A have shown that the glassy phase transition temperature is at about 800 °C.[35] Thus, between 1000 °C and 850 °C, the glassy phase solidifies progressively. As the glassy phase is in a liquid state above the Tg, it is assumed that a strong attenuation of the signals exists, linked to the evolution of the glassy phase viscosity. This phenomenon explains partially the progressive increase of cumulative signal energy and centroid frequency, i.e. the glassy phase behaves like a low-pass filter. Above the Tg, as the glassy phase is liquid, it can be assumed that microdamage mechanisms responsible for the narrow peak in Young's modulus evolution are mainly relative to rubbing phenomena between zirconia grains and the generation of zirconia variants with the associated intragranular microcracks. Observation of AE parameters shows that during the range 900–800 °C, the maximum of cumulative signal energy of the whole cooling process is observed whereas the centroid frequency only approaches its maximum value (it is only reached on the next temperature range 800–700 °C). A look at the number of cumulative hits on the different ranges of temperature in Table 1 is then of a great interest. In fact, it shows that the number of hits is half as important in the range 800–700 °C as in the range 700–600 °C.

If microdamage effects are probably dominant as soon as the glassy phase viscosity go through the Tg (between 800 °C and 700 °C), there is probably a mixing of intragranular microcracking phenomena, rubbing between grains and the glassy phase and rubbing between grains themselves. In the range 800–700 °C, it could switch to less intragranular microcracking phenomena and so the majority of signals could be created by rubbing phenomena. If the hypothesis is correct, it means that rubbing phenomena are less energetic but show more important centroid frequency than intragranular microcracks. This is consistent with the empirical bursting character of microcracks versus rubbing.

4.4.3.2. Medium temperature domain: 700–400 °C. A drop of centroid frequency and signal energy appears from 800–700 °C to 700–600 °C. This is accompanied by a large decrease of the number of hits. Then, signal energy and centroid frequency increase continuously between 700 °C and 400 °C. It can be seen at around 690 °C a loss of linearity which is considerably reinforced below 500 °C. At the same time, a slope change in the thermal expansion curve is observed at around 450 °C. This medium temperature range is probably the beginning of an other step of microdamage or coalescence of existing microcracks. In fact, since the glassy phase is completely solidified, CTE mismatches between zirconia grains and the glassy phase and between zirconia grains themselves are probably responsible for a progressive increasing of the stress field especially

Table 1
Number of cumulative hits associated to each 100 °C temperature domains during the cooling stage.

1000–900 °C	900–800 °C	800–700 °C	700–600 °C	600–500 °C	500–400 °C	400–300 °C	300–200 °C	200–100 °C
2327	7896	2981	1303	1123	1374	1280	1521	1136

around zirconia particles. As the number of hits is quite stable in this range, initiation mechanisms which are quick phenomena (lower centroid frequency) are maybe replaced by mechanisms of microcrack propagation and enlargement with higher energy and frequency parameters.

4.4.3.3. Low temperature range: 400–100 °C. The Young's modulus drops continuously down to 100 °C and no sensitive variation of cumulative signal energy or centroid frequency is recorded. Mechanisms of microcrack propagation follow in a regular way in the material. The material becomes more and more microdamaged.

5. Conclusion

Numerous materials are subjected to thermal treatments during their casting process. It is the case of refractory materials, in particular the fused-cast material with a high content of zirconia studied here. This study is a first approach to an understanding of microdamage mechanisms during high temperature treatments for an heterogeneous biphasic material. This paper shows the good reliability of an innovative acoustic emission device able to work up to 1500 °C and a procedure of data cleaning using an unsupervised pattern recognition. Then, the correlation of two chosen AE parameters – centroid frequency and signal energy – with elastic properties and thermal expansion data allows to establish hypothesis about the chronology of microdamage occurrence, even if it does not affect performance of materials at operating temperature for glass manufacturing because microcracks are for the most part recovered. In fact, both AE parameters can be interpreted as signature of microstructure mechanisms. Three domains of temperature have been highlighted to explain the way of intra and inter-microcracking happening, by taking into account the attenuation of the glassy phase due to its low viscosity at high temperature, the happening of the martensitic transformation of zirconia at around 1000 °C and the passage through the glassy phase transition at about 800 °C. A deeper investigation of defect identification requires to create a microcrack type and to identify directly its acoustic signature at a given temperature. This experiment is practically very hard to do. Nonetheless, this new AE system seems to be a powerful device to follow microstructure phenomena occurring during heat treatments and to complete thermo-mechanical characterizations. It could open the way to the development of more developed pattern recognition analysis using clustering approach during heat treatments in order to identify phase transformations or damage in composites or refractories. This approach illustrates an innovative way to go further in the understanding of microstructure changing occurring during a thermal treatment in a complex material.

Acknowledgements

Authors are greatly thankful to Saint-Gobain CREE for the furniture of the material, to the National Research Agency for the financial support and to Thierry Douillart (INSA Lyon) for ESEM observations.

References

1. Endo S, Hamaoka K, Ito A. Zirconia fused cast refractories. *Glass* 1990;**67**(3):109–13.
2. Ishino T. *Fusion cast refractories, refractories handbook*. Tokyo, Japan: The Technical Association of Refractory; 1998. pp. 201–209.
3. Boussuge M. Investigation of the thermomechanical properties of industrial properties: the French program PROMETHREF. *Eur Ceram Soc Bull* 2005.
4. Yeugo-Fogaing E, Huger M, Gault C. Elastic properties and microstructure: study of two fused cast refractory materials. *J Eur Ceram Soc* 2007;**27**(2–3):1843–8.
5. Lataste E. Microstructural and mechanical consequences of thermal cycles on a high zirconia fuse-cast refractory. *J Eur Ceram Soc* 2009;**29**(4):587–94.
6. Proust A, Lenain JC. Acoustic emission monitoring of civil infrastructures (Application of damage detection in full scale concrete structure). In: *EWGAE 2002 25th European Conference on Acoustic Testing*. 2002.
7. Hayakawa M, Kuntani M, Oka M. Structural study on the tetragonal to monoclinic transformation in arc-melted ZrO_2-2 mol.%Y_2O_3-I. Experimental observations. *Acta Metall* 1989;**37**(8):2223–8.
8. Hayakawa M, Oka M. Structural study on the tetragonal to monoclinic transformation in arc-melted ZrO_2-2 mol.%Y_2O_3-II. Quantitative analysis. *Acta Metall* 1989;**37**(8):2229–35.
9. Hayakawa M, Adachi K, Oka M. Crystallographic analysis of the monoclinic herringbone structure in arc-melted ZrO2-2 mol.%Y_2O_3 alloy. *Acta Metall Mater* 1990;**38**(9):1753–9.
10. Bakuckas JG, Prosser WH, Johnson WS. Monitoring damage growth in titanium matrix composites using acoustic emission. *J Comp Mater* 1994;**28**:305–28.
11. Berkovits A, Fang D. Study of fatigue crack characteristics by acoustic emission. *Eng Fract Mech* 1995;**51**:401–16.
12. Havlicek F, Crha J. Acoustic emission monitoring during solidification processes. *J Acoust Emis* 1999;**17**:3–4.
13. Barré S, Benzeggagh ML. On the use of acoustic emission to investigate damage mechanisms in glass-fiber-reinforced polypropylene. *Comp Sci Technol* 1994;**52**:369–76.
14. Chotard T, Rotureau D, Smith A. Analysis of the acoustic emission signature during aluminous cement setting to characterise the mechanical properties of the hard material. *J Eur Ceram Soc* 2005;**25**:3523–31.
15. Ersen A, Smith A, Chotard T. Effect of malic and citric acid on the crystallisation of gypsum investigated by coupled acoustic emission and electrical conductivity techniques. *J Mater Sci* 2006;**41**:7210–7.
16. Chotard T, Soro J, Lemercier H, Huger M, Gault C. High temperature characterisation of Cordierite-Mullite refractory by ultrasonic means. *J Eur Ceram Soc* 2008;**28**:2129–35.
17. Chotard T, Quet A, Ersen A, Smith A. Application of the acoustic emission technique to characterise liquid transfer in a porous ceramic during drying. *J Eur Ceram Soc* 2006;**26**:1074–84.
18. Avitavas N, Fowler T, Pothisiri T. Acoustic emission characteristics of pultruded fiber reinforced plastics under uniaxial tensile stress. In: *Proceedings of European WG on AE*. 2004. p. 447–54.
19. Yoon DJ, Weiss W, Shah SP. Assessing damage corroded reinforced concrete using in acoustic emission. *J Eng Mech* 2000:273–83.
20. Calabro A, Esposito C, Lizza A, Giordano M, D'Amore A, Nicolais S. Analysis of the acoustic emission signals associated to failure modes in CFRP laminates. *ECCM* 1997;**8**:425–32.
21. El Guerjouma R, et al. Non-destructive evaluation of damage and failure of fiber reinforced polymer composites using ultrasonic waves and acoustic emission. *Adv Eng Mater* 2001;**3**:601–8.
22. Ni QQ, Iwamoto M. Wavelet transform of acoustic emission signals in failure of model composites. *Eng Fract Mech* 2002;**69**:717–28.
23. De Groot PJ, Wijnen PAM, Janssen RBF. Real time frequency determination of acoustic emission for different fracture mechanisms in carbon/epoxy composites. *Comp Sci Technol* 1995;**55**:405–12.
24. Ferreira DBB, et al. Failure mechanism characterisation in composite materials using spectral analysis and the wavelet transform of acoustic emission signals. *INSIGHT* 2004;**46**(5):282–9.

25. Callego A, Gil GF, Vico JM, Ruzzante JE, Piotrkowsky R. Coating adherence in galvanized steel assessed by acoustic emission wavelet analysis. *Script Mater* 2005;**52**:1069–74.
26. Suzuki H, et al. Wavelet transform of acoustic emission signals. *J Acous Emiss* 1996;**14**:69–84.
27. Proust, A, Etude par la technique d'émission acoustique de la corrosion sous contrainte de 3 nuances d'acier inoxydable (Austénitique, Ferritique, Austénoferritique) en milieu chloruré chaud. Ph'D., Institut National des Sciences Appliquées de Lyon; 1992.
28. Pollock, AA, Acoustic emission from solids undergoing deformation. Ph'D, University of London; 1970.
29. Marec A, Thomas JH, El Guerjouma R. Damage characterisation of polymer-based composite materials: multivariable analysis and wavelet transform for clustering acoustic emission data. *Mech Syst Signal Process* 2008;**22**:1441–64.
30. Godin N, Huguet S, Gaertner R, Salmon L. Clustering of acoustic emission signals collected during tensile tests on unidirectional glass/polyester composites using supervised and unsupervised classifiers. *NDT&E Int* 2004;**37**:253–64.
31. Sause MGR, Haider F, Horn S. Quantification of metallic coating failure on carbon fiber reinforced plastics using acoustic emission. *Surf Coat Technol* 2009;**204**(3):300–8.
32. Bow S. *Pattern recognition-application to large data-set problems*. first ed. New-York: Marcel Dekker Inc.; 1984.
33. Philippidis TP, Nikolaidis V, Anastassopoulos AA. *NDT&E Int* 1998;**31**:329.
34. Likas A, Vlassis N, Verbeek J. The global k-means clustering algorithm. *Patt Recogn* 2003;**366**(2):451–61.
35. Patapy C, Gault C, Huger M, Chotard T. Acoustic characterization and microstructure of high zirconia electrofused refractories. *J Eur Ceram Soc* 2009;**29**(16):3355–62.